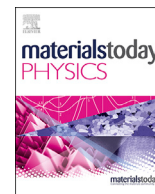




Contents lists available at ScienceDirect

Materials Today Physics

journal homepage: <https://www.journals.elsevier.com/materials-today-physics>

Pressure-induced enhancement of thermoelectric performance in palladium sulfide

Liu-Cheng Chen^{a, b, c}, Hao Yu^c, Hong-Jie Pang^c, Bin-Bin Jiang^{d, e}, Lei Su^f, Xun Shi^d, Li-Dong Chen^d, Xiao-Jia Chen^{c, *}

^a Key Laboratory of Materials Physics, Institute of Solid State Physics, Chinese Academy of Sciences, Hefei 230031, China

^b University of Science and Technology of China, Hefei 230026, China

^c Center for High Pressure Science and Technology Advanced Research, Shanghai 201203, China

^d State Key Laboratory of High Performance Ceramics and Superfine Microstructures, Shanghai Institute of Ceramics, Chinese Academy of Sciences, Shanghai 200050, China

^e University of Chinese Academy of Sciences, Beijing 100049, China

^f Key Laboratory of Photochemistry, Institute of Chemistry, Chinese Academy of Sciences, Beijing 100190, China

HPSTAR
572-2018



ARTICLE INFO

Article history:

Received 5 May 2018

Received in revised form

13 May 2018

Accepted 21 May 2018

Keywords:

Thermoelectricity

High pressure

Raman spectroscopy

Transport properties

ABSTRACT

Thermoelectric (TE) materials, which can directly convert waste heat into electric power, have attracted considerable interest because of their reliability and great potential for practical applications, especially in the current time faced with energy shortage. Recent advances in developing TE materials for power generation always optimize at high temperatures with the figure of merit (zT) above 1. However for the cooling or wearable devices, the high-efficiency TE materials with optimized temperature range near room temperature are strongly in demand. If the optimized TE performance can be tuned from high temperature to around room temperature, the extensive commercial application for microdevices could be expected. Here, we choose polycrystalline palladium sulfide as an example to show that pressure can significantly enhance the TE performance. With the measurements of the resistivity, Seebeck coefficient, and thermal conductivity under pressure up to 10 GPa, a times enhancement of the zT value has been obtained around room temperature. The largest value of zT at high pressures near 10 GPa is comparable to the value at ambient pressure near 800 K. The results indicate that pressure as an irreplaceable thermodynamic variable has positively regulated the TE performance around room temperature.

© 2018 Elsevier Ltd. All rights reserved.

Currently, the world is in thirst for green energy resources because of the excessive consumption relating to energy supply and environment. High-efficiency thermoelectric (TE) materials are an ideal system for power generation devices because of their ability to convert heat directly into electricity without producing unusable heat [1–3]. The effectiveness of a TE material is criticized by the dimensionless figure of merit (zT), which can be expressed as $zT = S^2 T \rho^{-1} \kappa^{-1}$, where S is the Seebeck coefficient, T is the absolute temperature, ρ is the electrical resistivity, and κ is the thermal conductivity, respectively. For TE devices, a conversion efficiency of at least 15% ($zT \geq 1$) is needed to reach the critical requirement, especially for the application in consumer markets [4]. With the increasing thirst for higher TE efficiency, many approaches have

been developed, such as (i) doping and alloying [4–7], (ii) variation in mesostructure [8], and (iii) band structure or lattice structure approaches [9–11]. However, there is still a long way to go to cross the theoretical zT value of 3 for broad applications because of the complex relationship of the three parameters (S , ρ , κ). In addition, recent advances in TE materials with $zT > 1$ for power generation are usually in mid-temperature (500–900 K) or high-temperature region (>900 K) [2,12]. However, the applications of thermoelectricity near room temperature are still hampered because of the lack of materials with zT above 1. Therefore, the room temperature TE materials with zT above 1 are urgently needed, especially in the applications of the micropower generators and microprocessors [13,14]. Unlike the temperature-turning effect (lattice expansion) on thermoelectricity, pressure-tuning may be a viable approach to change physical properties through lattice shrinking.

Pressure is a fundamental thermodynamic variable that can dramatically drive the modifications of crystal structure, electronic

* Corresponding author.

E-mail address: xjchen@hpcstar.ac.cn (X.-J. Chen).

structure, and magnetic structure of materials without introducing impurity, resulting in concomitant changes to their physical and chemical properties [15]. For TE materials, pressure tuning can not only change their TE performance but also offer a means to guide the search for higher zT [16]. From literature surveys, electrical resistivity usually has a better behavior at high pressures which is beneficial to the enhancement of zT [17,18]. Recently, measurements of Seebeck coefficient under pressure have been promoted by many experimental efforts, and the behavior of Seebeck coefficient under pressure is diversiform [19–21]. So far, little has yet been done to measure κ for TE materials under pressure. Here we choose a bulk material, palladium sulfide (PdS) as an example to demonstrate how applying pressure can tune and improve the TE performance based on the developed high-pressure techniques of Seebeck coefficient and thermal conductivity measurements.

PdS, which belongs to transition metal sulfides, has a tetragonal structure with the space group of $P4_2/m(84)$ (inset of Fig. 1a) and various interesting properties [22–25]. This binary PdS is a potential base thermoelectrical material with large power factor (PF) of $27 \mu\text{Wcm}^{-1}\text{K}^{-2}$ around 800 K at ambient pressure [26]. The high-pressure TE parameters of this sample have been collected based on the technique development using diamond anvil cells (DACs). The pressure dependent zT of this material around room temperature is

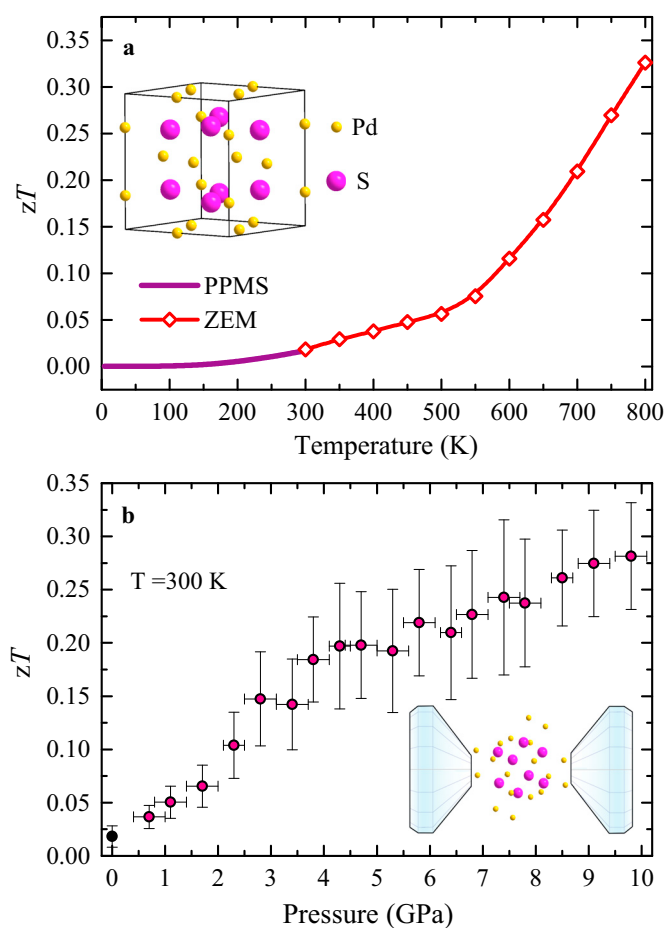


Fig. 1. (a) Temperature dependence of the dimensionless figure of merit zT of PdS at ambient pressure. The inset illustrates the crystal structure of the sample. (b) Pressure dependent zT of PdS around room temperature. Owing to the uncertainty in the measurements of the resistivity, Seebeck coefficient, and thermal conductivity under pressure, the error bars are very large for zT . PPMS, Physical Properties Measurement System, ZEM, Seebeck Coefficient / Electric Resistance Measurement System.

illustrated in Fig. 1b. The TE performance has a giant improvement at high pressures up to 4.5 GPa, and then slightly increases after passing a platform over a narrow pressure region. Obviously, the pressure-tuning effect on the TE performance of PdS has a nearly equivalent influence as the temperature-generated effect (Fig. 1a) [26]. In other words, the well-behaved TE performance of PdS at high temperature has been turned to room temperature by pressure effect. These results indicate that the route of applying pressure has successfully improved the TE performance of PdS around room temperature. Because some TE materials hold zT values around 0.5 at room temperature [1–3], one can expect the realization of zT to be above 3 if the similar pressure effects will be applied.

The detailed pressure dependence of the electrical conductivity, Seebeck coefficient, and thermal conductivity of PdS around room temperature is shown in Fig. 2. In all the experiments, pressure was obtained using DAC and was calibrated using the ruby fluorescence shift at room temperature [27]. All the results obtained under pressure are compared with the values measured at ambient pressure by Physical Properties Measurement System (PPMS) from Quantum Design. For the electrical conductivity (Fig. 2a), the detailed measurements can be seen elsewhere [25]. To give a more credible result, three separate temperature dependence of resistivity runs were carried out at various pressures. Some representative temperature dependent resistivity at various pressures (2.5, 5.6, and 9.5 GPa) are shown in Fig. 3. It can be seen that the resistivity of PdS is gradually suppressed with increasing pressure. The room temperature resistivity at different pressures is summarized in Fig. 2a. Obviously, the resistivity of PdS has a continuous decrease with increasing pressure (about two times). Resistivity for most semiconducting samples always decreases with increasing pressure due to the closing of the band gap [15]. A polynomial fitting is applied to the pressure-dependent resistivity. Then, the fitted results of resistivity are used to calculate zT values.

Based on the definition of the Seebeck coefficient $S = \Delta V / \Delta T$, we developed a high-pressure technique to measure S . The detailed setup diagram used for Seebeck coefficient measurement under pressure is shown in the inset of Fig. 2b. The temperature gradient (ΔT) from the heater to the cooler is measured by two separate W-Ta thin-film thermocouples connected with two digital temperature controllers [28]. The TE voltage (ΔV) along the temperature gradient is read out by a digital multimeter (218-A-5900, Keithley). The selected ΔV dependent of ΔT at the pressure of 0.7, 3.8, and 9.1 GPa is shown in Fig. 4. The Seebeck coefficient values are given by fitting the slopes of $\Delta V / \Delta T$, which are 384 ± 15 , 473 ± 14 , $414 \pm 10 \mu\text{V/K}$, respectively. All the relative errors of Seebeck coefficient are less than 10%. The obtained Seebeck coefficient as a function of pressure around room temperature is summarized in Fig. 2b. The S of PdS increases monotonously with increase pressure and reaches a maximum value of $473.0 \pm 30.5 \mu\text{V/K}$ at 3.8 GPa. After that, it has a continuous reduction with increasing pressure up to 10 GPa. Structure transition has not been observed up to 19 GPa [25]. Likely, the Seebeck coefficient hump around 3.8 GPa is associated with pressure-induced modulation of the band structure or electronic topological transition. The interrelationship between carrier concentration and Seebeck coefficient can be expressed as:

$$S = \frac{8\pi^2 k_B^2}{3eh^2} m^* T \left(\frac{\pi}{3n} \right)^{2/3},$$

where n is the carrier concentration and m^* is the effective mass of the carrier [2]. Therefore, one can conclude that the evolution of Seebeck coefficient at higher pressures is mainly caused by the increased carrier concentration. Similar behavior is not unusual in other samples [19–21]. Here, pressure is limited within 10 GPa for Seebeck coefficient measurements because of the unacceptable error of temperature at higher pressures.

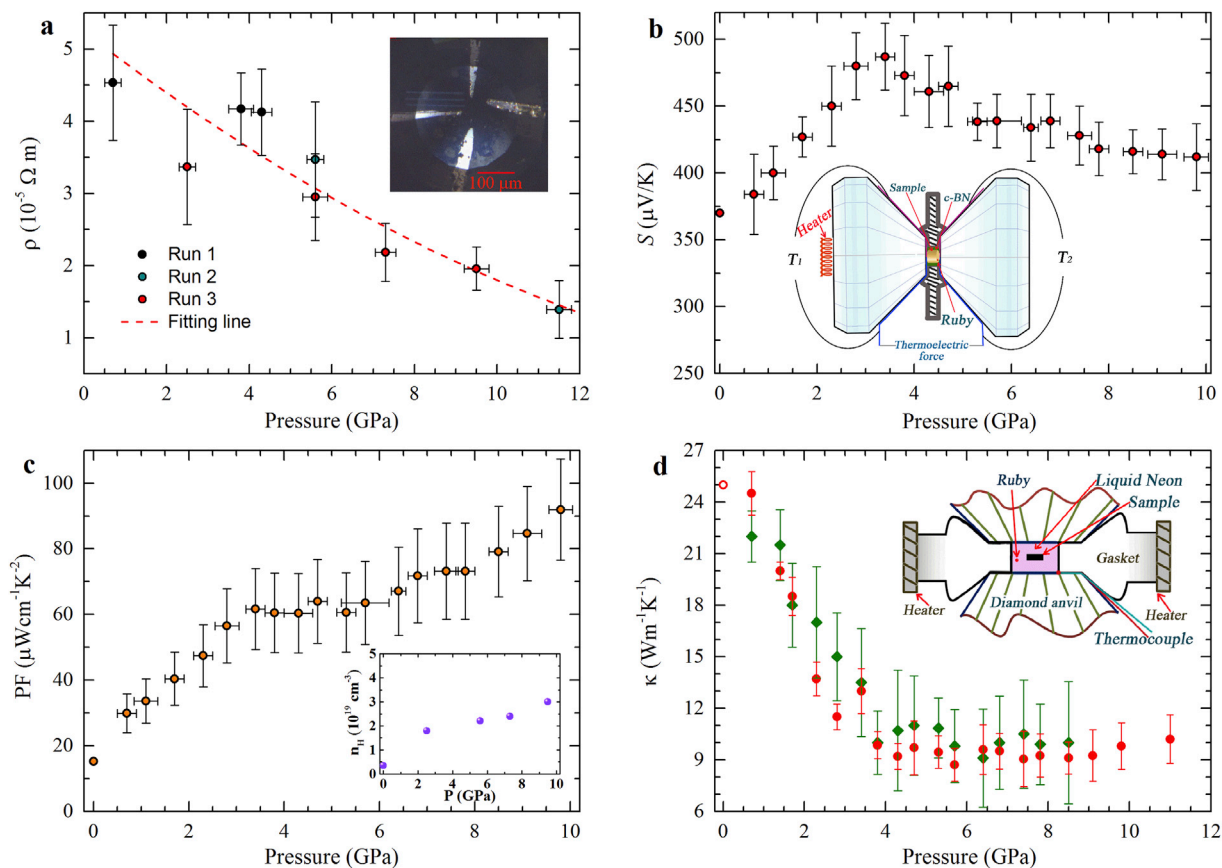


Fig. 2. (a) Pressure dependence of the electrical conductivity, (b) Seebeck coefficient, (c) power factor, and (d) thermal conductivity for PdS around room temperature. The red dotted line is the fitted resistivity according to the different resistivity runs. The insert of (a) shows the geometry of the four probes. Insert of (b): Diagram of Seebeck coefficient measurement under pressure. Insert of (c): Pressure dependent Hall carrier concentration at room temperature. Insert of (d): Diagram of thermal conductivity measurement under pressure. PF, power factor. (For interpretation of the references to color in this figure legend, the reader is referred to the Web version of this article).

The *PF* can be obtained by using the formula $PF=S^2/\rho$. The calculated results are plotted in Fig. 2c. Below 3.5 GPa, *PF* value has an obvious increase (nearly four times). Upon further compression, *PF* first exhibits a platform over a narrow pressure region of about 2 GPa and then increases again. The *PF* value at 9.7 GPa has about 7 times increase compared to the ambient pressure value. The significant improvement of *PF* is only realized by lattice compression. This incident adds evidence for the important role of pressure played in improving *PF* for TE materials [19,29].

To give the insight into the electrical properties of PdS under pressure, we performed the room temperature Hall effect measurement. The selected magnetic field-dependent Hall resistivity collected at room temperature is illustrated in Fig. 3. The inset of Fig. 2c shows the pressure-dependent carrier concentration *n* calculated by $n_H = 1/eR_H$, where *e* is the unit of the charge. Here *n_H* with the ideal value of 10^{19} cm^{-3} has a monotonous increase below the pressure of 10 GPa. Therefore, the pressure-induced optimization of *n_H* gives a reasonable explanation for the reduction of ρ , *S*, and the improvement of *PF*. This gives powerful evidence for the important role of pressure acted in optimizing the band structure and *n_H* for TE materials.

Until now, there have been only limited experimental data for thermal conductivity at high pressures because of the challenges in experiments. Here, an improved setup used for thermal conductivity measurement combined with micro-Raman scattering spectroscopy by changing temperatures and laser powers under pressure has been proposed. The setup diagram is shown in the

inset of Fig. 2d. The full Raman spectrum of PdS has been reported in our previous work [25]. The Raman signal was collected by a charge-coupled device (1024-PIXIS™100). Here the 330 cm^{-1} phonon mode is selected for thermal conductivity measurements because of its sensitivity to temperature and laser power changing. The results of pressure-dependent κ are summarized in Fig. 2d. It can be seen that κ has a continuous decrease with increasing pressure until the pressure around 4 GPa. After that, the values of κ almost remain the same with further compression.

The contactless methods for thermal conductivity detected under ambient pressure have been widely used in many materials with the help of micro-Raman scattering spectroscopy, such as porous silicon, graphene, and MoS₂ [30–33]. The frequencies of Raman modes always shift with the change of temperature due to the interaction of the related phonons and electrons. Thus, the local temperature rise induced by laser beam can be indirectly readout by the Raman shift. Dependent on the temperature- and laser power-dependent Raman measurements, the thermal conductivity can be evaluated by an original heat diffusion model expressed as [33]:

$$\kappa \frac{1}{r} \left[r \frac{dT(r)}{dr} \right] + q(r) = 0$$

where κ is the thermal conductivity, *T*(*r*) is the temperature distribution of the sample, *r* is the position measured from the beam center, and *q*(*r*) is the heat flux distribution from the heating point.

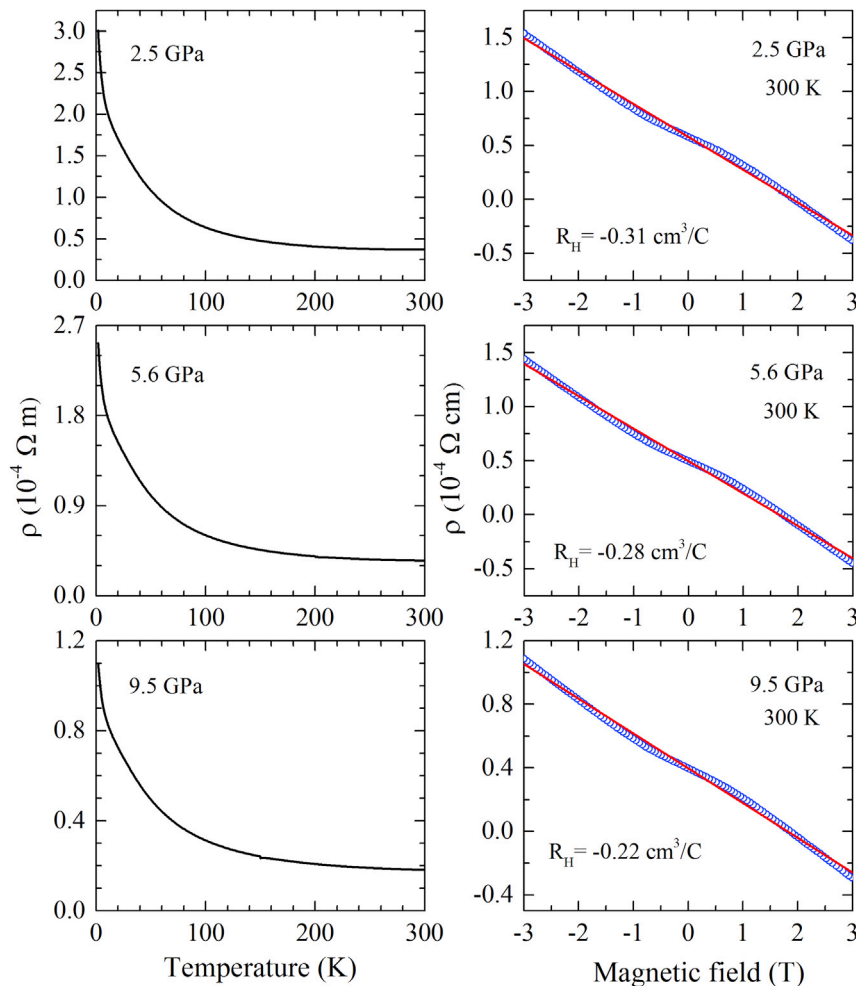


Fig. 3. Left: Representative temperature dependence of resistivity at the pressure of 2.5, 5.6, and 9.5 GPa. Right: Magnetic field dependence of the Hall resistivity measured at room temperature at the pressure of 2.5, 5.6, and 9.5 GPa.

The heat transfer of the sample with surround environment and the boundary conditions have been ignored in this model, and the isothermal surface is hemispheric. Dependent on this original heat diffusion model, a modified equation for thermal conductivity measured can be simplified as:

$$\kappa = \eta \frac{2W}{\pi\alpha\Delta T}$$

where W is the estimated laser power on the sample, η is the estimated laser absorption of the sample, α is the width of laser beam on the sample, ΔT is the temperature difference between the laser spot and the sample's edge. Generally speaking, the temperature (laser power) dependence of Raman modes can be linearly fitted by the equation $\omega_T = \omega_0 + \chi T$ ($\omega_W = \omega_0 + \chi W$), where χ is the first-order temperature (laser power) coefficient. Thus, the equation for calculating thermal conductivity can be further modified to reduce the systematic errors by the following equation:

$$\kappa = \eta \frac{2\Delta W/\Delta\omega}{\pi\alpha\Delta T/\Delta\omega} = \eta \frac{2\chi_T}{\pi\alpha\chi_W}$$

where $\Delta\omega$ is the phonon frequency shift due to the variation of temperature or laser power and χ_T (χ_W) is the first-order

temperature (laser power) derivative of ω . Considering the details of the previous studies [31–33], the main error sources in this method are the uncertainty of the optical absorption of the sample and the heat lost to the surrounding environment. In this article, the transition medium is liquid neon which has a very low thermal conductivity [34], at least two orders smaller than the polycrystalline PdS; thus, the heat transfer outside the sample can be ignored. The size of the sample is large enough, so the temperature increase at the boundary of sample caused by excitation laser is also neglected. The $20\times$ objective lens provides a Gaussian beam width, and α is estimated about $6\ \mu\text{m}$. The beam width is smaller than the radius of the sample at least one order, which could prevent the shallow heating on the layer of the sample induced by heat source. Here η is assumed to be insensitive to pressure and the assumption will not affect the studied trend with pressure. η is estimated from the comparison of the value of κ at ambient pressure measured by PPMS system and the method with the help of Raman scattering. Thus, we got the absorption coefficient of the sample in this Raman method which is about 0.5, and this absorption coefficient is also used for the thermal conductivity calculation at high pressures.

The phonon mode at around $330\ \text{cm}^{-1}$ is chosen as an example to show the details to calculate κ . As can be seen, this mode is very sensitive to temperature and laser power. The Raman spectra collected at three representative pressures (0.7, 4.3, and 9.8 GPa)

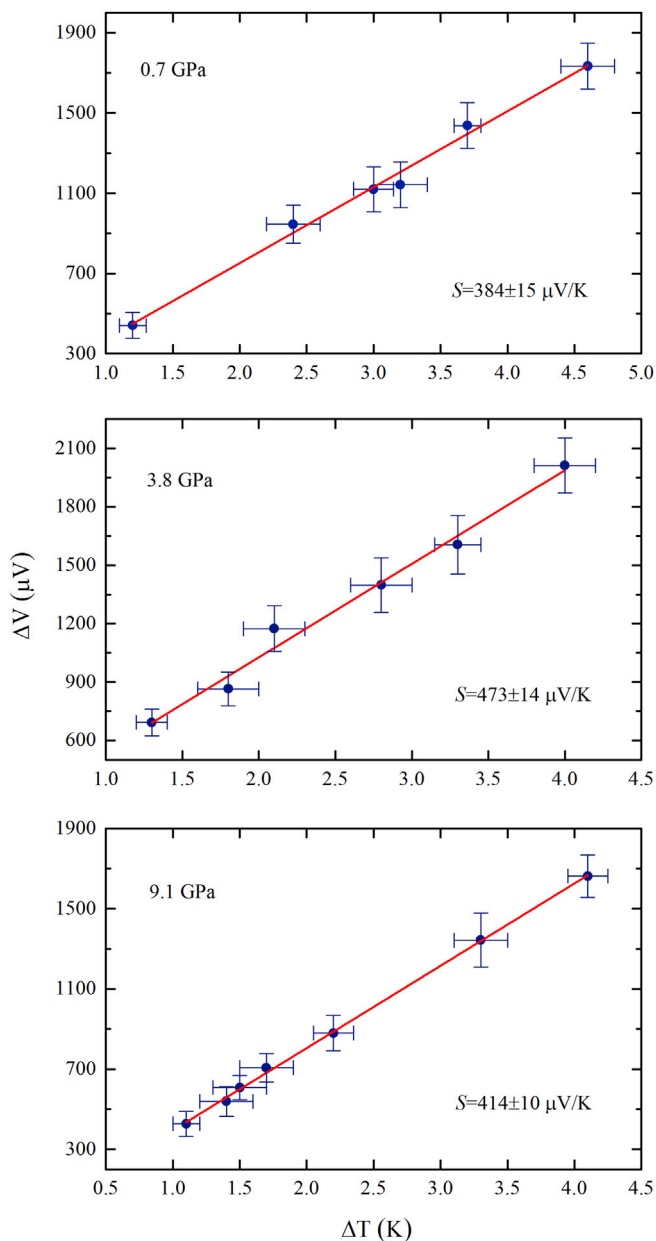


Fig. 4. The representative relationship between thermoelectric voltage (ΔV) and ΔT under the selected pressures of 0.7, 3.8, and 9.1 GPa. ΔT is limited within 5 K to reduce the relative errors of Seebeck coefficient.

are shown in Fig. 5. These spectra were collected either at different temperatures with a fixed laser power or by changing laser powers at a fixed temperature. The obtained frequencies as functions of temperature and laser power at various pressures (Fig. 6) were obtained by Lorentz fitting to the data. Then, χ_T and χ_W were determined by the linear fitting to the data for each pressure. Based on the measured α and the obtained η from the comparison of the ambient pressure κ value, we obtained the pressure dependence of κ for polycrystalline PdS (Fig. 1b).

The total thermal conductivity includes the lattice contribution κ_l and the electron contribution κ_e . The thermal conductivity from the lattice contribution is always determined by phonons transport in crystal, especially the low-frequency phonons. Raman scattering is a powerful tool in providing phonon information. The phonon

dispersion obtained from this technique is almost identical to that from neutron inelastic scattering [35–37]. We have examined the evolution of the low-frequency phonon mode around 60 cm^{-1} with pressure (Fig. 7). The phonon frequency and full width at half maximum (FWHM) were analyzed by Lorentz fitting to the data. The phonon frequency seemingly does not change too much with pressure, indicating that the mode Grüneisen parameter is weakly pressure dependent. However, there is a huge lattice contraction at pressures [15]. Therefore, the compressed lattice parameter might dominate the contribution to the changing trend of κ_l , slightly decreasing with increasing pressure and then saturating upon heavy compression. Notably, the FWHM first shows an increase and then keeps like a constant at high pressures. The increased FWHM implies a decrease of the lifetime of this phonon [38,39], which is consistent with the pressure-induced decrease of κ . The increase of FWHM can also be considered as the signature of the appearance of disorder in the crystal lattice [40]. It would increase phonon scattering and reduce the lattice thermal conductivity due to point defect scattering and also exhibit a possible broad Umklapp peak. The evolution of FWHM under pressure is synchronized with the pressure-induced changing trend of κ . These results indicate that the low-frequency phonon is indeed important in controlling the behavior of κ_l under pressure.

Having the knowledge of the significant enhancement of the TE efficiency by the applied pressure, one may wonder whether this effect can guide the synthesis and design of the sample at ambient pressure. It would be ideal if a material could maintain its high-pressure performance through some lattice modification but at ambient pressure. The almost same effect could be realized at least by the following ways: first, we suggest to grow ultrathin film on substrate with smaller lattice parameters. The lattice mismatch between the sample and substrate can introduce large compressive strain. The large enhancement of zT is expected due to the similarity between pressure and compressive strain. This idea has been proven to be very powerful in improving the physical properties in other systems. For example, compressive strain has been used to double the superconducting transition temperature in epitaxially grown ultrathin $\text{La}_{1.9}\text{Sr}_{0.1}\text{CuO}_4$ film [41,42]. The colossal magnetoresistance has also been realized at room temperature in ultrathin film through the compressive strain [43]. For the material with anisotropic uniaxial pressure effects, one can simulate the tensile and compressive strain along the different axial directions in ultrathin film [44]. Second, we propose to use the lattice distortion to introduce chemical pressure in the studied material. The significant change of the physical properties (particularly the change of superconducting transition temperature) has been observed in previous studies [45–47].

In summary, we have developed a series of techniques for the measurements of pressure dependence of the electrical conductivity, Seebeck coefficient, carrier concentration, and thermal conductivity. When collecting experimental data on a TE material PdS, we demonstrate that applying pressure is indeed an effective route to improve the TE performance. We find that the room temperature zT value of this material increases monotonously with pressure over the measured range. The obtained zT value of 0.28 ± 0.05 at room temperature and at 9.8 GPa is comparable to the value at high temperature of 800 K at ambient pressure. Because warming sample leads to the lattice expansion, applying pressure brings about the lattice compression. The realization of the almost same zT value by two opposite ways points to the great potential for the further improvement of the TE efficiency. The method for enhancing TE performance through lattice compression provides a lighthouse to improve zT value for these TE materials with high efficiency near room temperature.

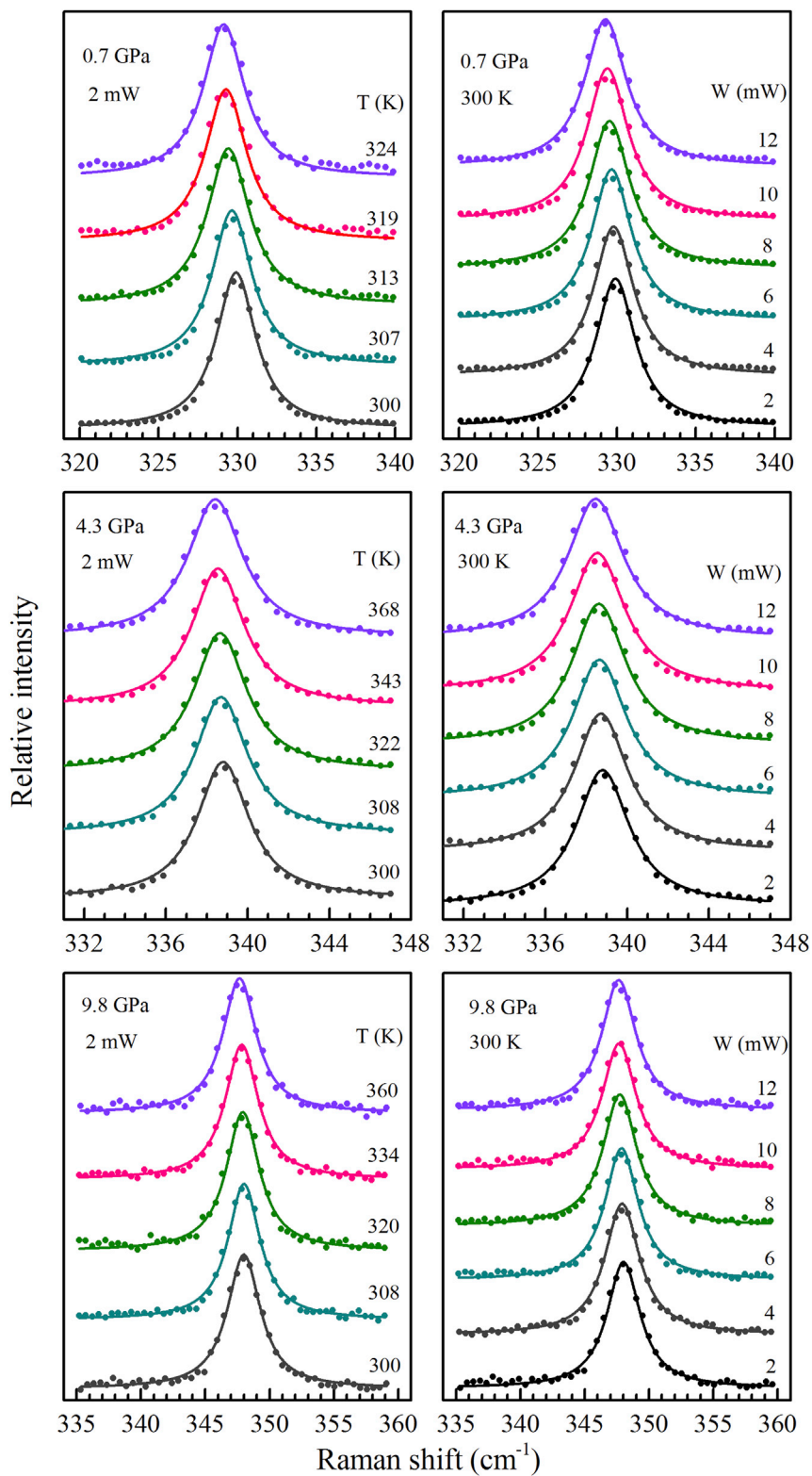


Fig. 5. Raman spectra of the 330 cm⁻¹ phonon mode as functions of temperature and laser power measured at pressure of 0.7, 4.3, and 9.8 GPa. The phonon frequencies were obtained by Lorentz fitting to the data.

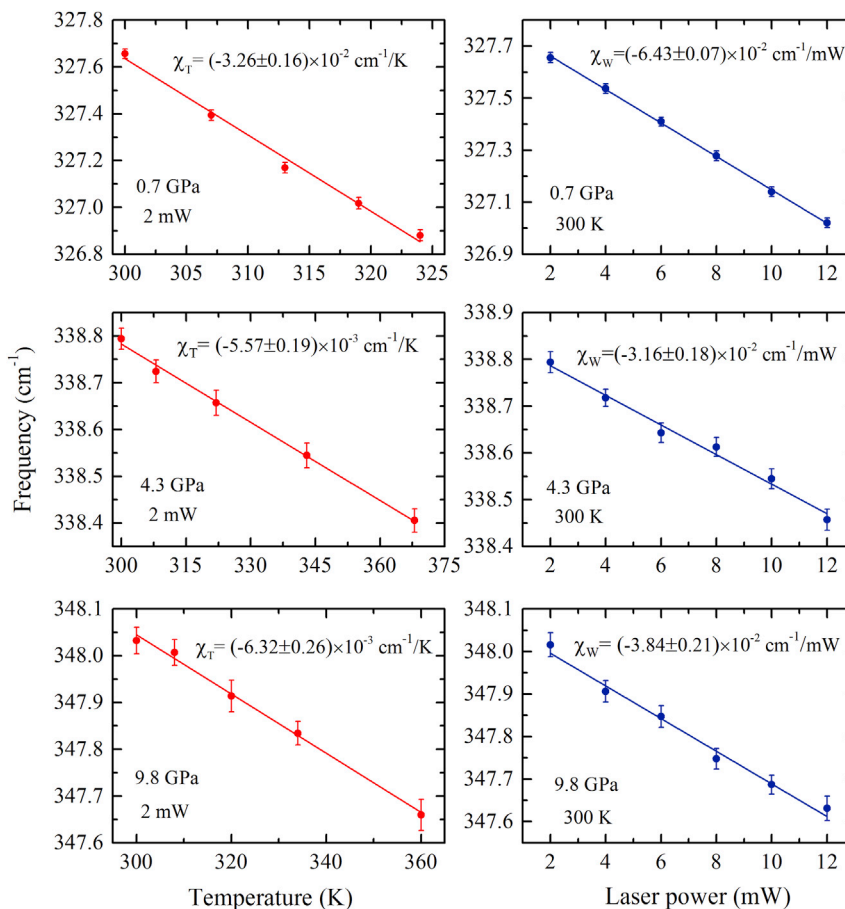


Fig. 6. Raman frequency of the 330 cm⁻¹ phonon mode as functions of temperature and laser power at pressure of 0.7, 4.3, and 9.8 GPa χ_T and χ_W were obtained from the linear fitting to the data.

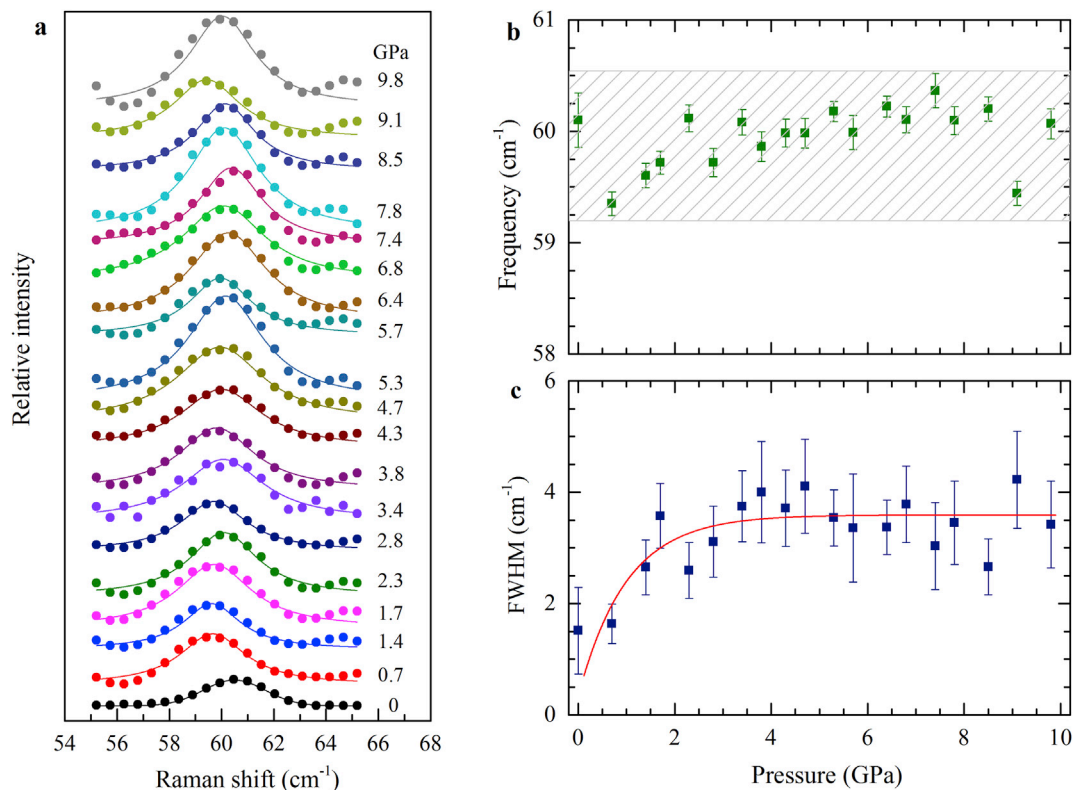


Fig. 7. (a) Raman spectra of the low-frequency phonon (60 cm⁻¹) at various pressures. The pressure dependence of the frequency and FWHM obtained through the fitting to the data with the help of Lorentz formula. (b) The dashed area represents the almost constant frequency over the studied pressure range. (c) Variation of the FWHM with pressure.

Acknowledgments

Lei Su acknowledged the support from the Natural Science Foundation of China (No. 21273206). Xun Shi and Li-Dong Chen acknowledged the support from the National Basic Research Program of China (973-program) under Project No. 2013CB632501, the Natural Science Foundation of China under the No. 11234012, and the Shanghai Government (Grant No. 15JC1400301).

References

- [1] G. Chen, M.S. Dresselhaus, G. Dresselhaus, J.P. Fleurial, T. Cailla, Recent developments in thermoelectric materials, *Int. Mater. Rev.* 48 (2003) 45–66.
- [2] G.J. Snyder, E.S. Toberer, Complex thermoelectric materials, *Nat. Mater.* 7 (2008) 105–114.
- [3] Z.F. Ren, Y.C. Lan, Q.Y. Zhang, *Advanced Thermoelectrics: Materials, Contacts, Devices, and Systems*, CRC Press, 2017.
- [4] W.S. Liu, J.Z. Hu, S.M. Zhang, M.J. Deng, C.G. Han, Y. Liu, New trends, strategies and opportunities in thermoelectric materials: a perspective, *Mater. Today Phys.* 1 (2017) 50–60.
- [5] J. Mao, Y.X. Wu, S.W. Song, J. Shuai, Z.H. Liu, Y.Z. Pei, Z.F. Ren, Anomalous electrical conductivity of *n*-type Te-doped $\text{Mg}_{3.2}\text{Sb}_{1.5}\text{Bi}_{0.5}$, *Mater. Today Phys.* 3 (2017) 1–6.
- [6] Z.H. Liu, J. Mao, S.Y. Peng, B.Q. Zhou, W.H. Gao, J.H. Sui, Y.Z. Pei, Z.F. Ren, Tellurium doped *n*-type $\text{Zr}_3\text{Ni}_3\text{Sb}_4$ thermoelectric materials: balance between carrier-scattering mechanism and bipolar effect, *Mater. Today Phys.* 2 (2017) 54–61.
- [7] R. He, H.T. Zhu, J.Y. Sun, J. Mao, H. Reith, S. Chen, G. Schierning, K. Nielsch, Z.F. Ren, Improved thermoelectric performance of *n*-type half-Heusler $\text{MCo}_{1-x}\text{Ni}_x\text{Sb}$ ($M = \text{Hf, Zr}$), *Mater. Today Phys.* 1 (2017) 24–30.
- [8] G. Rogl, P. Rogl, How nanoparticles can change the figure of merit, ZT, and mechanical properties of skutterudites, *Mater. Today Phys.* 3 (2017) 48–69.
- [9] J.P. Heremans, V. Jovicic, E.S. Toberer, A. Saramat, K. Kurosaki, A. Charoenphakdee, S. Yamanaka, G.J. Snyder, Enhancement of thermoelectric efficiency in PbTe by distortion of the electronic density of states, *Science* 321 (2008) 554–557.
- [10] Y.H. Wu, R.S. Zhai, T.J. Zhu, X.B. Zhao, Enhancing room temperature thermoelectric performance of *n*-type polycrystalline bismuth-telluride-based alloys via Ag doping and hot deformation, *Mater. Today Phys.* 2 (2017) 62–68.
- [11] K.P. Zhao, P.F. Qiu, Q.F. Song, A.B. Blichfeld, E. Eikeland, D.D. Ren, B.H. Ge, B.B. Iversen, X. Shi, L.D. Chen, Ultrahigh thermoelectric performance in $\text{Cu}_{2-y}\text{Se}_{0.5}\text{S}_{0.5}$ liquid-like materials, *Mater. Today Phys.* 1 (2017) 14–23.
- [12] X. Shi, L.D. Chen, C. Uher, Recent advances in high-performance bulk TE materials, *Int. Mater. Rev.* 61 (2016) 1–37.
- [13] G.J. Snyder, J.R. Lim, C.K. Huang, J.P. Fleurial, Thermoelectric microdevice fabricated by a MEMS-like electrochemical process, *Nat. Mater.* 2 (2003) 528–531.
- [14] N.S. Hudak, G.G. Amatucci, small-scale energy harvesting through thermoelectric, vibration, and radiofrequency power conversion, *J. Appl. Phys.* 103 (2008) 5–360.
- [15] H.K. Mao, X.J. Chen, Y. Ding, B. Li, L. Wang, Solids, liquids, and gases under high pressure, *Rev. Mod. Phys.* 90 (2018) 015007.
- [16] H. Yu, L.C. Chen, H.J. Pang, X.Y. Qin, P.F. Qiu, X. Shi, L.D. Chen, X.J. Chen, Impressive enhancement of thermoelectric performance in CuInTe_2 upon compression, *Mater. Today Phys.* 5 (2018) 1–6.
- [17] J.J. Ying, V.V. Struzhkin, Z.Y. Cao, A.F. Goncharov, H.K. Mao, F. Chen, X.H. Chen, A.G. Gavriliuk, X.J. Chen, Realization of insulating state and superconductivity in the Rashba semiconductor BiTeCl , *Phys. Rev. B* 93 (2016) 100504.
- [18] M.A. Hafez, X.M. Zhao, A.A. Kordyuk, Y.W. Fang, B. Pan, Z. He, C.G. Duan, J. Zhao, X.J. Chen, Enhancement of superconductivity under pressure and the magnetic phase diagram of tantalum disulfide single crystals, *Sci. Rep.* 6 (2016) 31824.
- [19] S.V. Ovsyannikov, V.V. Shchennikov, G.V. Vorontsov, A.Y. Manakov, A.Y. Likhacheva, V.A. Kulbachinskii, Giant improvement of thermoelectric power factor of Bi_2Te_3 under pressure, *J. Appl. Phys.* 104 (2008) 053713.
- [20] D.A. Polvani, J.F. Meng, N.V. Chandra Shekar, J. Sharp, J.V. Badding, Large improvement in thermoelectric properties in pressure-tuned *p*-type $\text{Sb}_{1.5}\text{Bi}_{0.5}\text{Te}_3$, *Chem. Mater.* 13 (2001) 2068–2071.
- [21] J.F. Meng, D.A. Polvani, C.D.W. Jones, F.J. DiSalvo, Y. Fei, J.V. Badding, Pressure tuning in the chemical search for improved thermoelectric materials: $\text{Nd}_x\text{Ce}_{3-x}\text{Pt}_3\text{Sb}_4$, *Chem. Mater.* 12 (2000) 197–201.
- [22] J.C.W. Folmer, J.A. Turner, B.A. Parkinson, Photoelectrochemical characterization of several semiconducting compounds of palladium with sulfur and/or phosphorus, *J. Solid State Chem.* 68 (1987) 28–37.
- [23] I.J. Ferrer, P. Díaz-Chao, A. Pascual, C. Sánchez, An investigation on palladium sulphide (PdS) thin films as a photovoltaic material, *Thin Solid Films* 515 (2007) 5783–5786.
- [24] M. Barawi, I.J. Ferrer, J.R. Ares, C. Sánchez, Hydrogen evolution using palladium sulfide (PdS) nanocrystals as photoanodes in aqueous solution, *ACS Appl. Mater. Inter.* 6 (2014) 20544–20549.
- [25] L.C. Chen, H. Yu, H.J. Pang, B.B. Jiang, L. Su, X. Shi, L.D. Chen, X.J. Chen, Pressure-induced superconductivity in palladium sulfide, *J. Phys. Condens. Matter* 30 (2018) 155703.
- [26] L.C. Chen, B.B. Jiang, H. Yu, H.J. Pang, L. Su, X. Shi, L.D. Chen, X.J. Chen, Thermoelectric properties of polycrystalline material palladium sulfide, *RSC Adv.* 8 (2018) 1–5.
- [27] H.K. Mao, P.M. Bell, J.W. Shaner, D.J. Stembey, Specific volume measurements of Cu, Mo, Pd, and Ag and calibration of the ruby R_1 fluorescence pressure gauge from 0.06 to 1 Mbar, *J. Appl. Phys.* 49 (1978) 3276.
- [28] J. Yang, M. Li, H.L. Zhang, C.X. Gao, Preparation of W-Ta thin-film thermocouple on diamond anvil cell for in-situ temperature measurement under high pressure, *Rev. Sci. Instrum.* 82 (2011) 045108.
- [29] L.Q. Xu, Y.P. Zheng, J.C. Zheng, Thermoelectric transport properties of PbTe under pressure, *Phys. Rev. B* 82 (2010) 195102.
- [30] S. Perichon, V. Lysenko, B. Remaki, D. Barbier, B. Champagnon, Measurement of porous silicon thermal conductivity by micro-Raman scattering, *J. Appl. Phys.* 86 (1999) 4700–4702.
- [31] S.S. Chen, A.L. Moore, W.W. Cai, J.W. Suk, J. An, C. Mishra, C. Amos, C.W. Magnuson, J.Y. Kang, L. Shi, R.S. Ruoff, Raman measurements of thermal transport in suspended monolayer graphene of variable sizes in vacuum and gaseous environments, *ACS Nano* 5 (2011) 321–328.
- [32] R.S. Yan, J.R. Simpson, S. Bertolazzi, J. Brivio, M. Watson, X.F. Wu, A. Kis, T.F. Luo, A.R. Hight Walker, H.G. Xing, Thermal conductivity of monolayer molybdenum disulfide obtained from temperature-dependent Raman spectroscopy, *ACS Nano* 8 (2014) 986–993.
- [33] N. Peimiyoo, J.Z. Shang, W.H. Yang, Y.L. Wang, C.X. Cong, T. Yu, Thermal conductivity determination of suspended mono- and bilayer WS_2 by Raman spectroscopy, *Nano Res.* 8 (2015) 1210–1221.
- [34] E. Löchtermann, Thermal conductivity of liquid neon, *Cryogenics* 3 (1963) 44–45.
- [35] C.W. Li, J. Hong, A.F. May, D. Bansal, S. Chi, T. Hong, G. Ehlers, O. Delaire, Orbital driven giant phonon anharmonicity in SnSe, *Nat. Phys.* 11 (2015) 1063–1069.
- [36] M. Christensen, A.B. Abrahamsen, N.B. Christensen, F. Juranyi, N.H. Andersen, K. Lefmann, J. Andreasson, C.R.H. Bahl, B.B. Iverse, Avoided crossing of rattler modes in thermoelectric materials, *Nat. Mater.* 7 (2008) 811–815.
- [37] X.J. Chen, V.V. Struzhkin, S. Kung, H.K. Mao, R.J. Hemley, A.N. Christensen, Pressure-induced phonon frequency shifts in transition-metal nitrides, *Phys. Rev. B* 70 (2004) 014501.
- [38] C. Ulrich, E. Anastassakis, K. Syassen, A. Debernardi, M. Cardona, Lifetime of phonons in semiconductors under pressure, *Phys. Rev. Lett.* 78 (1997) 1283–1286.
- [39] A.M. Hofmeister, Pressure dependence of thermal transport properties, *Proc. Natl. Acad. Sci. U.S.A.* 104 (2007) 9192–9197.
- [40] J.B. Zhang, V.V. Struzhkin, W.G. Yang, H.K. Mao, H.Q. Lin, Y.C. Ma, N.L. Wang, X.J. Chen, Effects of pressure and distortion on superconductivity in $\text{Tl}_2\text{Ba}_2\text{CaCu}_2\text{O}_{8+\delta}$, *J. Phys. Condens. Matter* 27 (2015) 445701.
- [41] J.P. Locquet, J. Perret, J. Fompeyrine, E. Mächler, J.W. Seo, G.V. Tendeloo, Doubling the critical temperature of $\text{La}_{1.9}\text{Sr}_{0.1}\text{CuO}_4$ using epitaxial strain, *Nature* 394 (1998) 453–456.
- [42] X.J. Chen, H.Q. Lin, Thickness dependence of the superconducting transition temperature of $\text{La}_{2-x}\text{Sr}_x\text{CuO}_4$ films, *Phys. Rev. B* 61 (2000) 9782–9785.
- [43] X.J. Chen, H.-U. Habermeier, H. Zhang, G. Gu, M. Varela, J. Santamaría, C.C. Almasan, Metal-insulator transition above room temperature in maximum colossal magnetoresistance manganite thin films, *Phys. Rev. B* 72 (2005) 104403.
- [44] X.J. Chen, H.Q. Lin, W.G. Yin, C.D. Gong, H.-U. Habermeier, Anisotropy of the superconducting transition temperature under uniaxial pressure, *Phys. Rev. B* 64 (2001) 212501.
- [45] J.P. Attfield, A.L. Kharlanov, J.A. McAllister, Cation effects in doped La_2CuO_4 superconductors, *Nature* 394 (1998) 157–159.
- [46] J.A. McAllister, J.P. Attfield, Systematic cation disorder effects in $\text{La}_{1.85}\text{M}_{0.15}\text{CuO}_4$ superconductors, *Phys. Rev. Lett.* 83 (1999) 3289–3292.
- [47] X.J. Chen, C.D. Gong, Y.B. Yu, Pressure effect on T_c for the rare-earth series $\text{RBa}_2\text{Cu}_3\text{O}_{7-\delta}$, *Phys. Rev. B* 61 (2000) 3691–3698.